

Flow of fluid of non-uniform viscosity in converging and diverging channels

By ALISON HOOPER,

School of Mathematics, Bristol University

B. R. DUFFY AND H. K. MOFFATT

Department of Applied Mathematics and Theoretical Physics,
Silver Street, Cambridge

(Received 17 February 1981 and in revised form 9 July 1981)

It is shown that the well-known Jeffery–Hamel solution of the Navier–Stokes equations admits generalization to the case in which the viscosity μ and density ρ are arbitrary functions of the angular co-ordinate θ . When $|R\alpha| \ll 1$, where R is the Reynolds number and 2α the angle of divergence of the planes, lubrication theory is applicable; this limit is first treated in the context of flow in a channel of slowly varying width. The Jeffery–Hamel problem proper is treated in §§ 3–6, and the effect of varying the viscosity ratio λ in a two-fluid situation is studied. In § 5, results already familiar in the single-fluid context are recapitulated and reformulated in a manner that admits immediate adaptation to the two-fluid situation, and in § 6 it is shown that the single-fluid limit ($\lambda \rightarrow 1$) is in a certain sense degenerate. The necessarily discontinuous behaviour of the velocity profile as the Reynolds number (based on volume flux) increases is elucidated. Finally, in § 7, some comments are made about the realizability of these flows and about instabilities to which they may be subject.

1. Introduction

Flows with non-uniform viscosity, particularly two-fluid flows with a viscosity jump at the interface, arise in many processes of technological importance. Analysis of such problems is complicated (i) by the fact that the interface geometry in general changes with time even if the boundary conditions are steady, and (ii) by the fact that, if the interface intersects a solid boundary, the no-slip condition is (in general) inadequate in an immediate neighbourhood of the contact line, which may be observed to move relative to the solid surface.

In attempting to approach problems in this category in a general way, it seems natural first to study situations in which these particular difficulties are avoided. Figure 1 shows one such situation, viz the flow of a fluid of non-uniform viscosity along a two-dimensional duct of slowly varying width. This elementary problem is analysed (under the lubrication approximation) in § 2, in order to provide motivation for the subsequent study (§§ 3–7) of the Jeffery–Hamel configuration (figure 2), which is the main content of this paper. In § 3, we show that the well-known exact solution of the Navier–Stokes equations (Jeffery 1915, Hamel 1916; see Batchelor 1967, § 5.6) can be generalized to the situation in which the viscosity μ and/or the density ρ are

arbitrary functions of the angular co-ordinate θ —conditions that are clearly compatible with a steady purely radial flow. A continuous variation of μ and ρ can be induced by heating one boundary, and in this case (§ 3) an exact solution of the coupled nonlinear equations of motion and heat transfer may be obtained.

In §§ 4–6, we specialize to the two-fluid problem of figure 2(c), in which the density is continuous, but the viscosity is discontinuous across $\theta = 0$. In § 4, the low-Reynolds-number analysis for this situation is presented, and the upper limit of the angle 2α for which purely radial flow may be expected is obtained. In § 5, results that are well-known for the uniform viscosity case are obtained by a numerical procedure and are interpreted in a new light. In § 6, the same numerical procedure is used to analyse the effects of the viscosity jump, and it emerges that an important effect of the viscosity stratification is to resolve the degeneracy implied by the possible existence of steady asymmetric solutions which (in the uniform-viscosity case) are mirror images of each other. Resolution of this degeneracy also implies important qualitative changes in the behaviour of the flow as the Reynolds number increases.

2. Flow of viscosity-stratified fluid in a slowly varying channel

In the situation of figure 1(a), let α be a typical wall slope, and let $R = Q\rho/\bar{\mu}$, where $2Q$ is the total flux of fluid, and $\bar{\mu}$ is the average viscosity across the channel. Then we may expect that the lubrication approximation will be valid provided that

$$\alpha \ll 1, \quad R\alpha \ll 1. \quad (2.1)$$

The natural transverse co-ordinate is

$$\eta = \frac{y + a_2(x)}{a_1(x) + a_2(x)} \quad (0 \leq \eta \leq 1), \quad (2.2)$$

and, in the lubrication approximation, the streamlines are given by $\eta = \text{const.}$ A steady flow is possible if μ is constant on streamlines, i.e. if

$$\mu = \mu(\eta). \quad (2.3)$$

The velocity $u(\eta)$ along the streamlines then satisfies

$$\frac{1}{a^2} \frac{\partial}{\partial \eta} \left(\mu \frac{\partial u}{\partial \eta} \right) = -G(x), \quad (2.4)$$

where

$$G(x) = -\partial p / \partial x, \quad a(x) = a_1(x) + a_2(x). \quad (2.5)$$

With boundary conditions $u(0) = u(1) = 0$, (2.4) integrates to give

$$u(\eta) = -a^2 G \int_0^\eta (\eta_1 - \bar{\eta}) \mu^{-1}(\eta_1) d\eta_1, \quad (2.6)$$

where

$$\bar{\eta} = \int_0^1 \eta \mu^{-1} d\eta / \int_0^1 \mu^{-1} d\eta. \quad (2.7)$$

In the two-fluid case shown in figure 1(b), the interface $y = h(x)$ becomes $\eta = H$, where

$$\frac{a_1 - h}{a_2 + h} = \frac{1 - H}{H}, \quad (2.8)$$

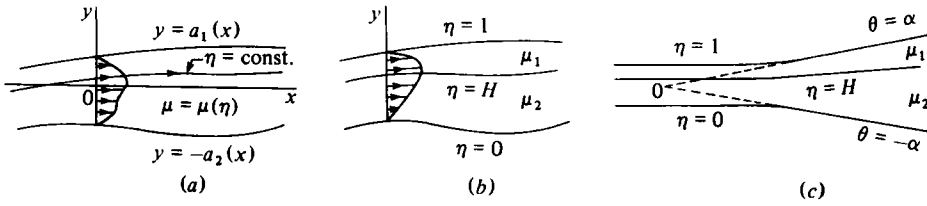


FIGURE 1. Flow in a slowly varying channel with viscosity stratification: (a) continuous variation of viscosity; (b) two-layer model; (c) two layers entering a slowly diverging section; the interface positions itself in the diverging section along a plane $\theta = \text{const.}$

i.e. the ratio of widths of the two layers is constant. The viscosity function is

$$\mu(\eta) = \begin{cases} \mu_1 & (\eta > H), \\ \mu_2 & (\eta < H), \end{cases} \tag{2.9}$$

and, from (2.7),

$$2\bar{\eta} = \frac{1 + (\lambda - 1)H^2}{1 + (\lambda - 1)H}, \quad \lambda = \frac{\mu_1}{\mu_2}. \tag{2.10}$$

In the lower fluid (viscosity μ_2), (2.6) gives

$$u = u_2(\eta) = \frac{a^2 G}{\mu_2} (\eta\bar{\eta} - \frac{1}{2}\eta^2), \tag{2.11}$$

and the flux in this layer is

$$Q_2 = a \int_0^H u_2(\eta) d\eta = \frac{a^3 G}{6\mu_2} (3\bar{\eta} - H) H^2. \tag{2.12}$$

Similarly,

$$Q_1 = \frac{a^3 G}{6\mu_1} (3\bar{\eta}' - (1 - H)) (1 - H)^2, \tag{2.13}$$

where (cf. 2.10)

$$2\bar{\eta}' = \frac{1 + (\lambda^{-1} - 1)(1 - H)^2}{1 + (\lambda^{-1} - 1)(1 - H)}. \tag{2.14}$$

Clearly, since Q_1 and Q_2 are both constant, we must have

$$a^3 G = \text{const.} \tag{2.15}$$

Moreover, elimination of $a^3 G$ from (2.12) and (2.13) yields

$$\lambda q H^2 [\lambda H^2 + (1 - H)(3 + H)] = (1 - H)^2 [(1 - H)^2 + \lambda H(4 - H)] \tag{2.16}$$

(where $q = Q_1/Q_2$), a quartic equation for H , which has a unique real root $H(q, \lambda)$ in the physically relevant range $0 < H < 1$.

We have neglected surface tension in the above analysis. The pressure jump due to surface tension γ is approximately $\gamma \partial^2 h / \partial x^2$, and the associated jump in pressure gradient along the interface is $\gamma \partial^3 h / \partial x^3$. If, for example, $h(x) = h_0 \cos kx$, with $\alpha = h_0 k$, this jump has order of magnitude $\gamma \alpha^3 / h_0^2$, and this is negligible compared with $|\partial p / \partial x| \sim \bar{\mu} Q / a_0^3$ (where a_0 is a typical value of $a(x)$) provided that

$$\alpha^3 \ll \frac{\bar{\mu} Q}{\gamma a_0} \left(\frac{h_0}{a_0} \right)^2. \tag{2.17}$$

For very slow flow rates, surface tension inevitably becomes important, and will tend to keep the interface plane in the situation sketched in figure 1(b).

For the particular case of a channel that diverges at a constant angle (figure 1(c),

the condition (2.8) implies that the streamlines in the diverging section are purely radial ($\theta = \text{const.}$ in polar co-ordinates with origin $r = 0$ at the (virtual) intersection of the diverging planes). Hence, in the diverging section, $\mu = \mu(\theta)$, and $u \propto f(\theta)/r$, from mass conservation. The above simple analysis is of course valid only if the conditions (2.1) are satisfied.

In §3, we relax these conditions, and consider the general Jeffery–Hamel problem for arbitrary α and R , and arbitrary $\mu(\theta)$. We shall also allow the density ρ to be a function of θ ; since inertia is, in general, important, this will also have an influence on the velocity field.

3. Jeffery–Hamel flow with $\mu = \mu(\theta)$, $\rho = \rho(\theta)$

Consider now the flow configuration of figure 2(a), with $\mu = \mu(\theta)$, $\rho = \rho(\theta)$. Let

$$\bar{\mu} = \frac{1}{2\alpha} \int_{-\alpha}^{\alpha} \mu(\theta) d\theta, \quad \bar{\rho} = \frac{1}{2\alpha} \int_{-\alpha}^{\alpha} \rho(\theta) d\theta, \quad (3.1)$$

and let $\tilde{\mu}(\theta) = \mu/\bar{\mu}$, $\tilde{\rho}(\theta) = \rho/\bar{\rho}$. In polar co-ordinates (r, θ, z) , let

$$\mathbf{u} = 2 \frac{\bar{\mu}}{\bar{\rho}} \left(\frac{f(\theta)}{r}, 0, 0 \right). \quad (3.2)$$

Then the radial and transverse components of the Navier–Stokes equations are

$$\frac{\bar{\rho}}{\bar{\mu}^2} \frac{\partial p}{\partial r} = \frac{1}{r^3} [2(\tilde{\mu}f')' + 4\tilde{\rho}f^2], \quad \frac{\bar{\rho}}{\bar{\mu}^2} \frac{\partial p}{\partial \theta} = \frac{4}{r^2} (\tilde{\mu}f)', \quad (3.3)$$

where $p(r, \theta)$ is the pressure field. From the second of these,

$$\frac{\bar{\rho}}{\bar{\mu}^2} (p - p_0) = \frac{1}{r^2} (4\tilde{\mu}f - c), \quad (3.4)$$

where c is constant, and p_0 is at most a function of r . Substitution in (3.3a) shows that p_0 may be taken to be constant, and we obtain

$$(\tilde{\mu}f')' + 4\tilde{\mu}f + 2\tilde{\rho}f^2 = c. \quad (3.5)$$

This is the required generalization of the standard Jeffery–Hamel equation

$$f'' + 4f + 2f^2 = c. \quad (3.6)$$

The boundary conditions are

$$f = 0 \quad \text{on} \quad \theta = \pm\alpha, \quad (3.7)$$

and it follows from (3.3) and (3.5) that

$$c = [(\tilde{\mu}f')']_{\theta=\pm\alpha} = \frac{\bar{\rho}}{2\bar{\mu}^2} \left(r^3 \frac{\partial p}{\partial r} \right)_{\theta=\pm\alpha}. \quad (3.8)$$

The constant c therefore provides a measure of the wall pressure gradient.

If $f(\theta, \alpha, c, \Lambda)$ is any solution of (3.5), (3.7), where the ‘parameter’ Λ summarizes the dependence on the functions $\tilde{\mu}(\theta)$ and $\tilde{\rho}(\theta)$,† then we may construct a corresponding Reynolds number

$$R = Q\bar{\rho}/\bar{\mu} = \int_{-\alpha}^{\alpha} f(\theta, \alpha, c, \Lambda) d\theta = R(\alpha, c, \Lambda), \quad (3.9)$$

where $R > 0$ corresponds to (net) diverging flow, and $R < 0$ corresponds to (net) converging flow. For fixed α , (3.9) provides a relationship (in effect) between wall pressure gradient (i.e. c) and flow rate (i.e. R).

† Strictly, of course, this is a functional dependence.

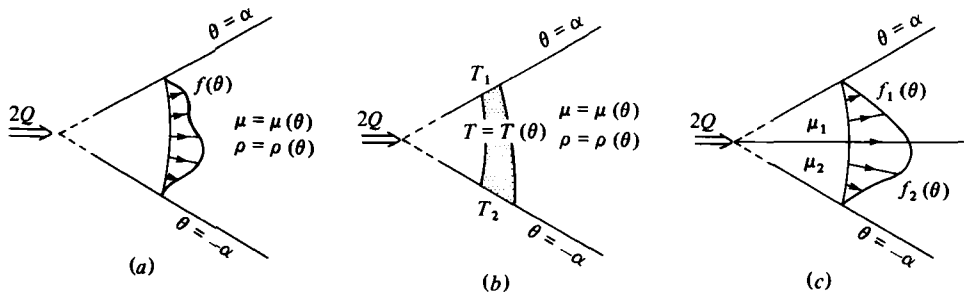


FIGURE 2. The Jeffery-Hamel configuration: (a) source flow ($Q > 0$) or sink flow ($Q < 0$) with angular stratification of μ and ρ ; (b) angular stratification caused by differential heating of the boundaries $\theta = \pm \alpha$; (c) the two-layer flow studied in §§ 4 and 6.

In the well-studied case of a single fluid of homogeneous properties, the parameter Λ of course disappears and we have a relationship

$$R = R(\alpha, c), \tag{3.10}$$

which defines a surface (with possibly many folds and branches) in the space of the variables (R, α, c) . The geometry of this surface provides important information both about the multiplicity of steady-state solutions and about the manner in which a solution changes as α or R is slowly varied. A classification of velocity profiles in terms of the numbers of maxima and minima that they exhibit was provided by Rosenhead (1940) and refined by Fraenkel (1962), who then sought to determine the boundaries in the (R, α) -plane of regions in which solutions of a given class may exist. This information is in fact all contained in the function (3.10); for example, the important ‘barrier’ curves $\mathcal{B}_3, \mathcal{B}_{-2}$ of Fraenkel (1962) may in principle be obtained by eliminating c between (3.10) and the equation

$$g(\alpha, c) \equiv \partial R / \partial c = 0. \tag{3.11}$$

In § 5 below, we shall recapitulate some results of the single-fluid analysis, and present these in a manner that admits simple extension to the inhomogeneous situation.

Before specializing to the two-fluid problem, let us briefly note one situation in which continuous angular stratification of viscosity and density may be expected, viz that in which the walls $\theta = \pm \alpha$ are maintained at different temperatures T_1 and T_2 , as depicted in figure 2 (b). A steady temperature distribution $T(r, \theta)$ is then established in the fluid. Neglecting buoyancy forces, the velocity field is still given by (3.2), and, neglecting heat produced by viscous dissipation,† T satisfies

$$\mathbf{u} \cdot \nabla T = \kappa \nabla^2 T, \tag{3.12}$$

where κ is the thermal diffusivity of the fluid. The solution is simply

$$T = (T_1 - T_2) \theta / 2\alpha + \frac{1}{2}(T_1 + T_2), \tag{3.13}$$

and so μ and ρ , being functions of T , are functions of θ via (3.13). When $\Delta T = T_1 - T_2$ is not too large, a linear variation of μ and ρ with θ may be expected.

The neglected buoyancy force is of order $\alpha_T g \Delta T$, where α_T is the coefficient of

† The heating effect associated with viscous dissipation in the uniform-viscosity case was studied by Millsaps & Pohlhausen (1953).

thermal expansion, and this is indeed negligible compared with the viscous force (of order $\nu|Q|/r^3$) provided

$$r \ll (\nu|Q|/\alpha_T g \Delta T)^{\frac{1}{2}} = r_b. \quad (3.14)$$

Neglect of viscous heating Φ is justified if the extra temperature $T_v(r, \theta)$ generated in this way is small compared with ΔT . Considering only the case of converging flow ($Q < 0$), T_v is given (in order of magnitude) by

$$\frac{Q}{r} \frac{\partial T_v}{\partial r} \sim \Phi \sim \frac{\bar{\mu}}{\rho c_p} \frac{Q^2}{r^4},$$

i.e.

$$T_v \sim \bar{\mu}|Q|/\rho c_p r^2,$$

and so $T_v \ll \Delta T$ provided

$$r \gg (\bar{\mu}|Q|/\rho c_p \Delta T)^{\frac{1}{2}} = r_a. \quad (3.15)$$

Both inequalities (3.14) and (3.15) can be satisfied provided that

$$\bar{\mu}|Q| \alpha_T^2 g^2 / \rho c_p^3 \Delta T \ll 1, \quad (3.16)$$

and, under this condition, μ and ρ will be functions only of θ throughout the range $r_a \ll r \ll r_b$.

4. Discontinuous variation of μ ; behaviour near $R = c = 0$

To simplify matters, suppose now that ρ is uniform, and that μ is uniform except for a discontinuity on the plane $\theta = 0$ (figure 2c):

$$\mu = \begin{cases} \mu_1 & (0 < \theta < \alpha), \\ \mu_2 & (-\alpha < \theta < 0). \end{cases} \quad (4.1)$$

Then $\bar{\mu} = \frac{1}{2}(\mu_1 + \mu_2)$, and, writing

$$f(\theta) = \begin{cases} f_1(\theta) & (0 < \theta \leq \alpha), \\ f_2(\theta) & (-\alpha \leq \theta < 0), \end{cases} \quad (4.2)$$

(3.5) becomes

$$\bar{\mu}_1(f_1'' + 4f_1) + 2f_1^2 = c = \bar{\mu}_2(f_2'' + 4f_2) + 2f_2^2, \quad (4.3)$$

and we have the boundary conditions

$$f_1(\alpha) = f_2(-\alpha) = 0, \quad (4.4)$$

$$[f]_{-}^{+} = [\mu f']_{-}^{+} = 0 \quad \text{on} \quad \theta = 0, \quad (4.5)$$

the latter ensuring continuity of velocity and tangential stress across the interface. It may be noted that the normal stress is

$$\sigma_{\theta\theta} = -p + 2\mu e_{\theta\theta} = -p + 2\bar{\mu}\tilde{\mu} \left(\frac{2\bar{\mu}}{\rho} \right) \frac{f}{r^2}, \quad (4.6)$$

and this is automatically continuous across $\theta = 0$ since the constant c in (3.4) is the same throughout the flow domain.

We consider first the behaviour near $R = c = 0$, where the terms $2f_1^2$, $2f_2^2$ of (4.3) may (presumably) be neglected. The solution of (4.3)–(4.5) is then

$$\left. \begin{aligned} c^{-1}f_1(\theta) &= A(\cos 2\alpha - \cos 2\theta) + B(\sin 2\alpha - \sin 2\theta), \\ c^{-1}f_2(\theta) &= \lambda C(\cos 2\alpha - \cos 2\theta) - \lambda B(\sin 2\alpha + \sin 2\theta), \end{aligned} \right\} \quad (4.7)$$

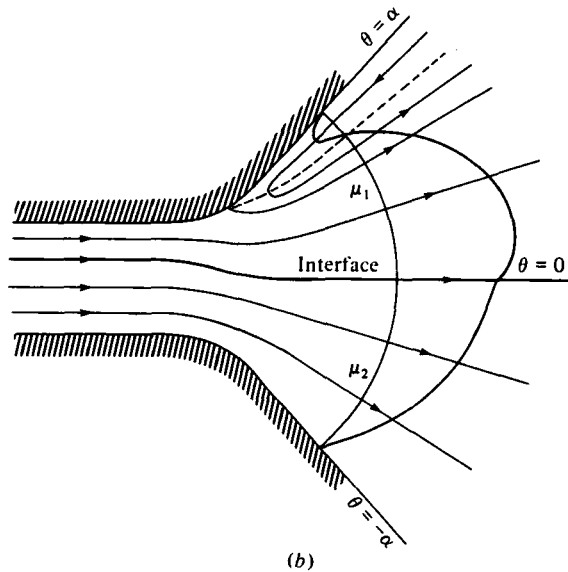
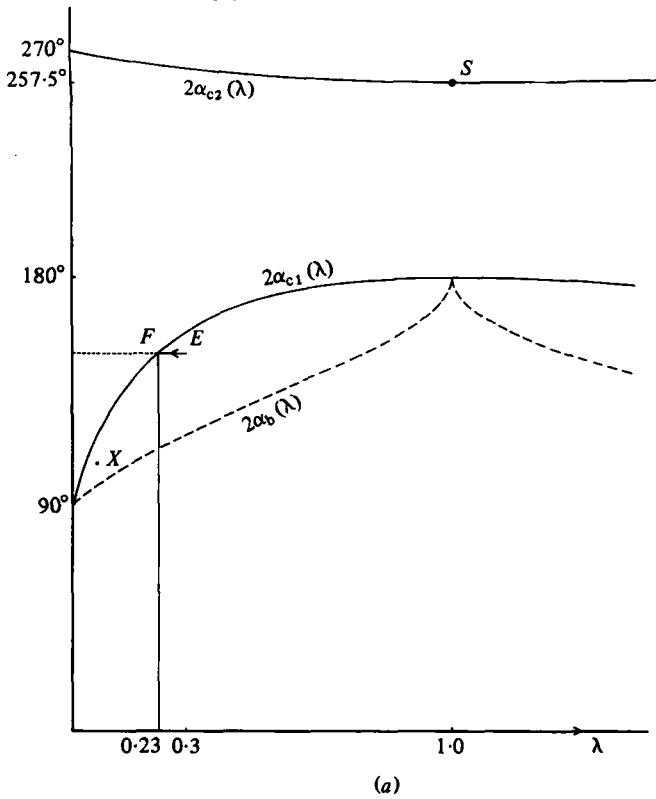


FIGURE 3. (a) Curves given by (4.11) (solid) and (4.12) (dashed). Above the dashed curve, reversed flow occurs in the less viscous fluid. On the solid curve $2\alpha_{c1}(\lambda)$, the inertia-free solution (4.7) is singular; for $\alpha > \alpha_{c1}(\lambda)$, eigenfunction solutions dominate over the Jeffery-Hamel solution; the point S ($\lambda = 1, 2\alpha \simeq 257.5^\circ$) is singular in this respect. The change in the character of the (R, c) -diagram along the segment $E \rightarrow F$ is discussed in § 6. (b) Sketch showing the low-Reynolds-number streamline pattern that may be expected at a point such as X of figure 3(a) (where reversed flow occurs) when a channel diverges at an angle 2α .

where

$$A = \frac{2\lambda + (1-\lambda)\cos 2\alpha}{8\lambda\cos 2\alpha}, \quad B = \frac{(1-\lambda)(1-\cos 2\alpha)}{8\lambda\sin 2\alpha}, \quad C = \frac{2-(1-\lambda)\cos 2\alpha}{8\lambda\cos 2\alpha}, \quad (4.8)$$

and $\lambda = \mu_1/\mu_2 (= \tilde{\mu}_1/\tilde{\mu}_2)$. The Reynolds-number relation (3.9) may then be calculated in the form

$$R/c = (8\lambda)^{-1}[(\lambda-1)^2(\alpha - \tan \alpha) + 2\lambda(2\alpha - \tan 2\alpha)] = g(\alpha, \lambda), \quad \text{say}, \quad (4.9)$$

and we may infer that the general function $R(\alpha, c, \lambda)$ satisfies

$$(\partial R/\partial c)_{c=R=0} = g(\alpha, \lambda). \quad (4.10)$$

There is a singular behaviour when $g(\alpha, \lambda) = 0$, i.e. when

$$\frac{\tan 2\alpha - 2\alpha}{\tan \alpha - \alpha} = -\frac{(\lambda-1)^2}{2\lambda}. \quad (4.11)$$

For any $\lambda > 0$, there are two angles $\alpha_{c_1}(\lambda)$ and $\alpha_{c_2}(\lambda)$ satisfying (4.11); these are shown by the solid curves of figure 3(a). Only the lower curve $2\alpha_{c_1}(\lambda)$ is in general physically relevant,† since the similarity solution loses physical significance for $\alpha > \alpha_{c_1}(\lambda)$; in this regime, the flow may be expected to be sensitive to the precise geometry and entry conditions near O (Barenblatt & Zel'dovich 1972; Moffatt & Duffy 1980).

As the angle 2α increases from zero, the wall stress as given by the solution (4.7) decreases, and vanishes first (in the less viscous fluid) when $(\partial f/\partial \theta)_{\theta=\alpha} = 0$; this condition determines an angle α_b given by

$$\cos 2\alpha_b = \frac{-2\lambda}{1+\lambda}. \quad (4.12)$$

The variation of $2\alpha_b$ with λ is shown by the dashed curve of figure 3(a). For $2\alpha > 2\alpha_b$, reversed flow occurs in the less-viscous fluid. The streamlines may then be expected to have the form sketched in figure 3(b).

5. Recapitulation and reformulation of results for the single-fluid situation ($\lambda = 1$)

5.1. Analytical results

There are three independent analytical results that provide useful checks on the numerical procedure that follows.

(i) *Inertia-free limit.* When $\lambda = 1$, (4.9) gives

$$R/c = \frac{1}{4}(2\alpha - \tan 2\alpha), \quad (5.1)$$

from which we infer that

$$(\partial R/\partial c)_{R=c=0} = \frac{1}{4}(2\alpha - \tan 2\alpha). \quad (5.2)$$

Note that the slope of the (R, c) -curve at the origin changes sign as 2α increases through $\frac{1}{2}\pi$.

† The single-fluid limit $\lambda \rightarrow 1$ is peculiar here; the symmetric low- R flow breaks down (Fraenkel 1962) at $2\alpha_{c_2}(1) \simeq 257.5^\circ$. For the two-fluid flow ($\lambda \neq 1$), the velocity is necessarily asymmetric about $\theta = 0$, and it is the antisymmetric ingredient that produces the singularity on the lower curve when $\lambda \neq 1$. (The limits $\lambda \rightarrow 1$ and $2\alpha \rightarrow \pi$ do not commute.)

(ii) *Rosenhead's exact solution.* A particular exact solution of (3.6) and (3.7) (Rosenhead 1940, equation (5.11)) is given by

$$f(\theta) = 2H - 1 - 3H \tanh^2 H^{\frac{1}{2}}\theta, \tag{5.3}$$

where H is a parameter related to α by

$$\alpha H^{\frac{1}{2}} = \operatorname{artanh} \left(\frac{2H - 1}{3H} \right)^{\frac{1}{2}}, \tag{5.4}$$

the corresponding values of c and R then being

$$c = 2(H^2 - 1), \quad R = 2[3(2H - 1)]^{\frac{1}{2}} - 2\alpha(H + 1). \tag{5.5}$$

Equation (5.4) has two roots $H_1(\alpha)$ and $H_2(\alpha)$ for $\alpha < \alpha_0 \simeq 38 \cdot 23^\circ$. When $\alpha = \alpha_0$, these solutions merge, and there is no real solution for $\alpha > \alpha_0$. Equations (5.4), (5.5) define (parametrically) a curve in the (α, c, R) -space which lies on the surface $R = R(\alpha, c)$ in the region $R > 0, \alpha \leq \alpha_0$. Figure 4 shows the projection of this curve on the (c, R) -plane, the trajectories of the two solutions as α increases from 0 to α_0 being as indicated. (When $\alpha = \alpha_0, H \simeq 1 \cdot 198, R \simeq 1 \cdot 159, c \simeq 0 \cdot 868$.) The projection of the same curve on the (R, α) -plane is the curve denoted \mathcal{B}_1 by Fraenkel (1962).

When $H \gg 1$, (5.4) gives

$$\alpha H^{\frac{1}{2}} \sim \operatorname{artanh} \left(\frac{2}{3} \right)^{\frac{1}{2}} = 1 \cdot 146\dots = \beta, \quad \text{say,} \tag{5.6}$$

and (5.5) gives

$$\alpha R \sim 2\beta(\sqrt{6} - \beta) = 2 \cdot 988\dots, \quad H \sim \left(\frac{1}{2}c \right)^{\frac{1}{2}} \gg 1. \tag{5.7}$$

Equation (5.3) may then be written

$$f(\theta) \sim H\{2 - 3 \tanh^2 [H^{\frac{1}{2}}(\alpha - \theta) - \beta]\}, \tag{5.8}$$

which has the character of a positive jet trapped between the two walls.

(iii) *Boundary-layer behaviour as $c \rightarrow \infty$.* When c is large, (3.6) may be solved by boundary-layer techniques. For a boundary layer on $\theta = \alpha$, the appropriate boundary-layer variable is

$$\eta = K(\alpha - \theta), \quad K = \left(\frac{1}{2}c \right)^{\frac{1}{2}}, \tag{5.9}$$

and f admits the asymptotic expansion†

$$f(\theta) \sim K^2 f_0(\eta) + f_1(\eta) + K^{-2} f_2(\eta) + \dots \tag{5.10}$$

The appropriate boundary conditions are

$$f_n(0) = 0, \quad f'_n(\eta) \rightarrow 0 \quad \text{as} \quad \eta \rightarrow \infty \quad (n = 0, 1, 2, \dots). \tag{5.11}$$

Substitution of (5.10) in (3.6) gives, at leading order,

$$f''_0 = 2(1 - f_0^2), \quad f_0(0) = 0, \quad f'_0(\infty) = 0, \tag{5.12}$$

with the well-known solution (see e.g. Goldstein 1938, § 56)

$$f_0 = 2 - 3 \tanh^2 (\eta + \beta), \tag{5.13}$$

† An expansion of this kind was proposed by Bulakh (1964), but he did not obtain the solution (5.15) for f_1 obtained here.

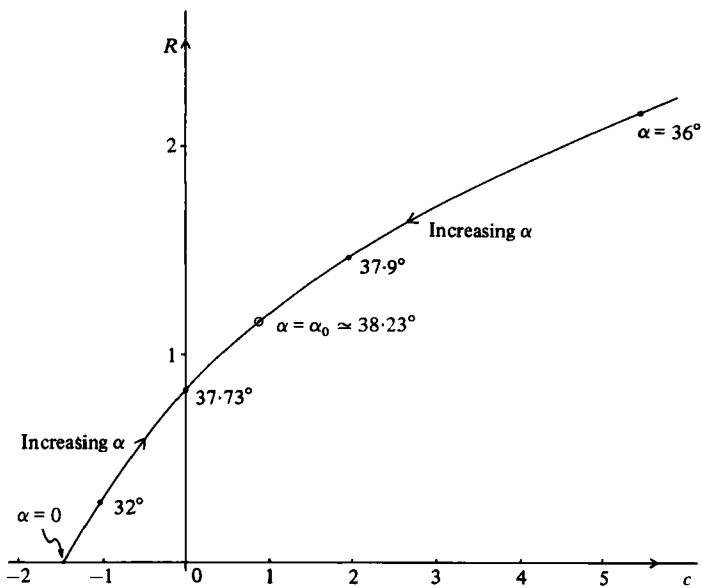


FIGURE 4. Locus of the Rosenhead solution (5.3)–(5.5) as α increases from 0 to α_0 .

where $\beta \simeq 1.146$ as above. At the next order,

$$f_1'' + 4f_0(f_1 + 1) = 0, \quad f_1(0) = 0, \quad f_1'(\infty) = 0, \tag{5.14}$$

and this has the solution

$$f_1 = 3\left(\frac{3}{2}\right)^{\frac{1}{2}} \tanh(\eta + \beta) \operatorname{sech}^2(\eta + \beta) - 1. \tag{5.15}$$

From (3.9) we now have

$$R = 2 \int_0^\alpha f(\theta) d\theta \sim \frac{2}{K} \int_0^{K\alpha} (K^2 f_0 + f_1) d\eta,$$

or, in terms of c ,

$$R \sim -\alpha(2c)^{\frac{1}{2}} + 6\left(1 - \left(\frac{3}{2}\right)^{\frac{1}{2}}\right) \left(\frac{1}{2}c\right)^{\frac{1}{2}} - 2\alpha + \left(\frac{3}{2}\right)^{\frac{1}{2}} \left(\frac{2}{c}\right)^{\frac{1}{2}} + O(c^{-\frac{1}{2}}). \tag{5.16}$$

Higher terms in this expansion may be obtained, but the expression (5.16) is quite sufficient to provide a good check on the accuracy of the numerical procedure (see figures 6 and 7 below).

Two other types of asymptotic solution may be constructed, and these are also relevant in cataloguing possible behaviour for large c . These are the ‘wall-jet boundary-layer’ solution (cf. (5.8))

$$f_J \sim K^2[2 - 3 \tanh^2(\eta - \beta)] - [3\left(\frac{3}{2}\right)^{\frac{1}{2}} \tanh(\eta - \beta) \operatorname{sech}^2(\eta - \beta) + 1] + O(K^{-2}), \tag{5.17}$$

and the ‘interior-jet’ solution

$$f_I \sim K^2[3 \operatorname{sech}^2 K(\theta - \theta_1) - 1] - 1 + O(K^{-2}). \tag{5.18}$$

The latter makes a contribution to R given by

$$\delta R_J \sim \int_{-\alpha}^\alpha (f_J + K^2 + 1) d\theta \sim 6K, \tag{5.19}$$

so that, for example, a velocity profile exhibiting a single central jet with conventional boundary layers on both walls will yield an asymptotic relationship only slightly different from (5.16), namely

$$R \sim -\alpha(2c)^{\frac{1}{2}} + 6(2 - (\frac{2}{3})^{\frac{1}{2}})(\frac{1}{2}c)^{\frac{1}{2}} - 2\alpha + (\frac{2}{3})^{\frac{1}{2}}\left(\frac{2}{c}\right)^{\frac{1}{2}} + O(c^{-\frac{1}{2}}). \quad (5.20)$$

5.2. Numerical results

Accurate determination of any of the characteristics of the surface $R = R(\alpha, c)$ requires numerical work, either using the exact elliptic-function solution of Rosenhead (1940), or by direct numerical integration of (3.6). The latter procedure is more easily extendable to the inhomogeneous situation, and it is therefore the procedure that we adopted. The equation was integrated by a shooting method, using a fourth-order Runge-Kutta-Merson procedure. For given c , $f'(-\alpha)$ was guessed, and the equation integrated across to $\theta = \alpha$. According to the value of $f(\alpha)$, $f'(-\alpha)$ was then modified, and the integration repeated. The procedure was iterated until the condition $f(\alpha) = 0$ was satisfied to a specified accuracy.

The linearized solution provided a guide in the initial guess-work for small c ; and then, for each new value of c , linear extrapolation gave a first estimate of the new $f'(-\alpha)$. For each solution $f(\theta, \alpha, c)$, the corresponding $R = R(\alpha, c)$ was calculated from (3.9). Figure 5 shows the form of the resulting curves near the origin ($R = c = 0$) for $2\alpha = \frac{1}{2}\pi$, $\frac{3}{2}\pi$ and π . The slope of the tangent at the origin satisfies (5.2), and the point X corresponding to Rosenhead's solution for $2\alpha = \frac{1}{2}\pi$ is as indicated. Points on these curves (which we shall denote as *branch A curves*) correspond to solutions which, in a sense elaborated by Fraenkel (1962), are analytically dependent on R and α in a neighbourhood of $R = 0$ and $\alpha = 0$.

Figure 6 shows the branch A curve for $2\alpha = \frac{1}{2}\pi$ computed out to $c = 300$. This shows three important features, which are present also in similar diagrams for all other values of $\alpha < \alpha_c$ (for the behaviour when $\alpha > \alpha_c$, see § 5.3 below):

(i) The solid curve corresponds to solutions symmetric about $\theta = 0$, while the dashed curve that branches off from the point P_a corresponds to solutions that are asymmetric about $\theta = 0$. At P_a , $f'(\pm\alpha) = 0$, and as we pass through P_a on the solid curve, reversed flow appears on both walls. In Fraenkel's notation, for different values of α , the value of R , $= R_P(\alpha)$ say, at P_a provides the curve \mathcal{B}_2 (for $2\alpha < \pi$) and \mathcal{B}_{-1} (for $2\alpha > \pi$). The bifurcation at P_a from symmetric to asymmetric flows is continuous (but not analytic) in the parameter R .

(ii) The solid curve shows a maximum at the point R_a ($R_a \simeq 5.5$ in figure 6). For $R > R_a$, a steady solution analytically related to the branch A solutions is not possible. Since $\partial R/\partial c = 0$ at R_a , it is clear that, as stated earlier, the corresponding 'barrier' in the (R, α) -plane is given by eliminating c between (3.10) and (3.11). If R is increased through $R_a(\alpha)$, discontinuous behaviour *must* occur (see below).

(iii) For $R < 0$ and c large, the asymptotic expansion (5.16) is relevant; the 1-term, 2-term, 3-term and 4-term approximations are as indicated in figure 6; the 4-term approximation is indistinguishable from the exact numerical curve for $c \gtrsim 20$. Similarly, the circled points on the upper solid portion of branch A (figure 6) have been calculated from (5.20) to order $c^{-\frac{1}{2}}$, and the accuracy here is good for $c \gtrsim 200$; the profiles here do indeed have the character of a forward central jet with reversed flow near the walls. For $c \simeq 200$ ($K \simeq 3.16$) and $\alpha = \frac{1}{2}\pi$, the second term of (5.20) evidently

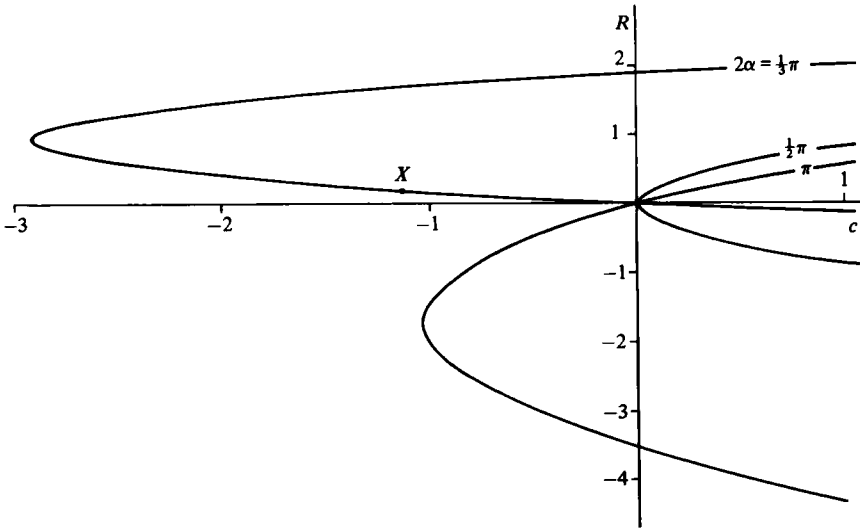


FIGURE 5. Branch A curves near $R = c = 0$ for $2\alpha = \pi, \frac{1}{2}\pi, \frac{1}{3}\pi$. Rosenhead's solution corresponds to the point X on the curve $2\alpha = \frac{1}{3}\pi$ ($c = -1.131, R = 0.217$).

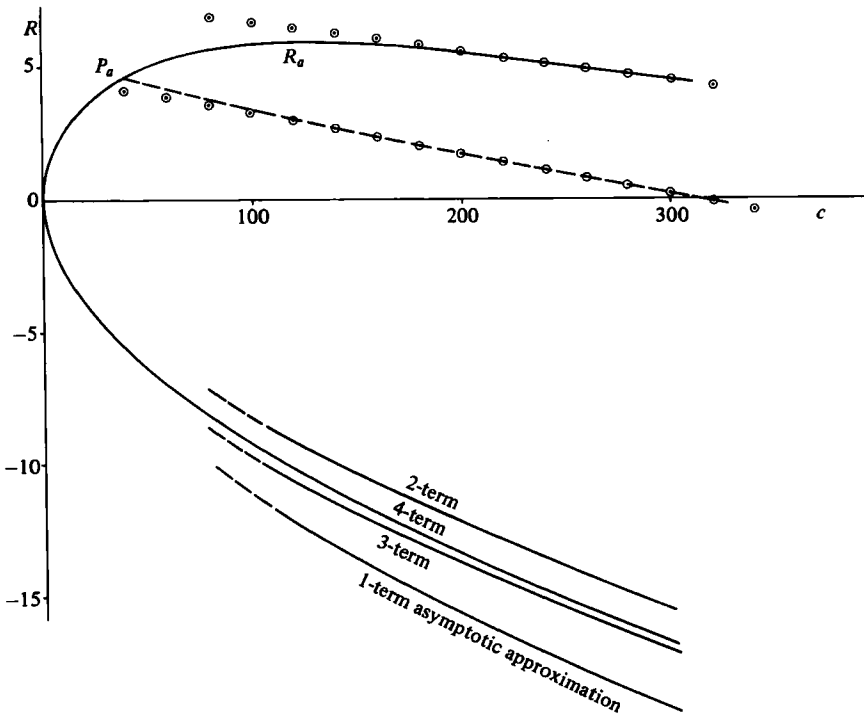
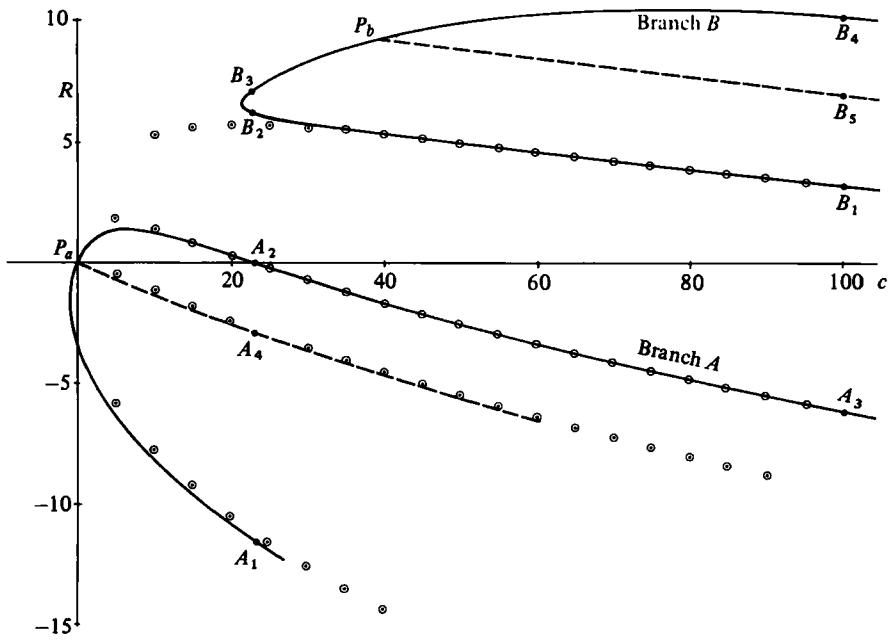
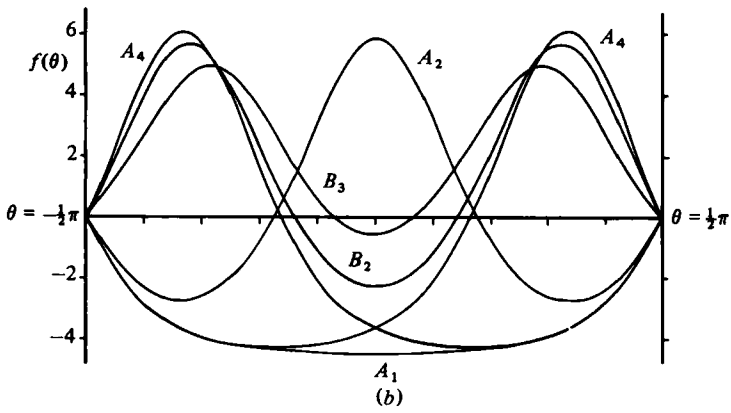


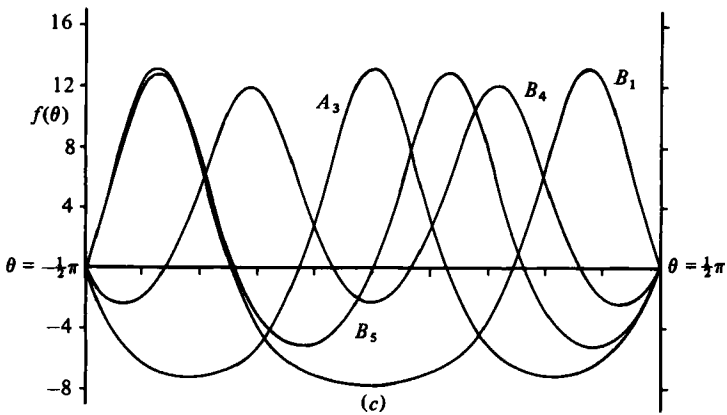
FIGURE 6. Branch A of the curve $R = R(\frac{1}{3}\pi, c)$, together with successive approximations to the lower portion based on the asymptotic expansion (5.16). The four-term approximation is indistinguishable from the exact result for $c \gtrsim 20$ ($-R \gtrsim 5$). The circled points are values predicted by the asymptotic results of §5.1, correct to order $c^{-\frac{1}{2}}$.



(a)

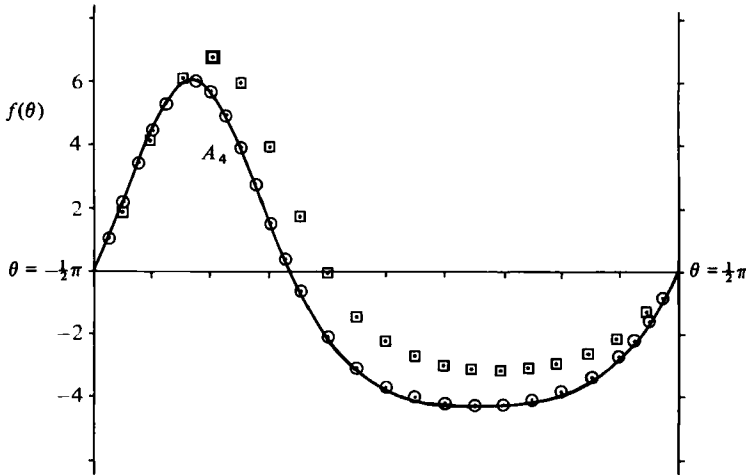


(b)



(c)

FIGURE 7(a, b, c). For legend see p. 296.



(d)

FIGURE 7. (a) The function $R = R(\frac{1}{2}\pi, c)$; the solid portions correspond to flows symmetric about $\theta = 0$, and the dashed portions correspond to asymmetric flows. The circled points are values predicted by the asymptotic analyses. (b) Velocity profiles corresponding to the points A_1, A_2, A_4, B_2 and B_3 . (c) Velocity profiles corresponding to points A_3, B_1, B_4, B_5 . Only one of the two asymmetric profiles B_5 is included here. (d) Asymmetric velocity profile A_4 ($c = 23, R = -2.5$) and points calculated from one-term (\square) and two-term (\circ) boundary-layer analysis.

still dominates over the first, and so $R > 0$. The points on the dashed portion of branch A have been evaluated through combining a normal boundary layer on one wall with a 'wall-jet boundary layer' (equation (5.17)) on the other.

The question of what may happen when $R > R_a$ is to some extent answered by figure 7(a), which shows the (R, c) -diagram for $2\alpha = \pi$. This shows a second computed branch, denoted *branch B*, which extends to higher positive values of R . The velocity profiles corresponding to the points A_1, \dots, A_4 on branch A , and B_1, \dots, B_5 on branch B are shown in figures 7(b,c). The circled points in figure 7(a) again correspond to asymptotic evaluation correct to order $c^{-\frac{1}{2}}$. The points on the lower portion of branch B were obtained using a wall-jet boundary layer on each wall (see e.g. the profile labelled B_1 in figure 7(c)). The profile A_4 (figure 7d) (a wall-jet on one boundary and a conventional boundary layer on the other) is poorly approximated by the leading-order boundary-layer analysis, but accurately represented when the $O(1)$ terms of (5.10) and (5.17) are included. If R increases through R_a , then clearly a jump to branch B is possible, such a jump involving a 30-fold increase in c ! This is a transition, in Fraenkel's (1962) notation, from a profile of class II_2 to a profile of class III_2 ; the fact that it is necessarily discontinuous was recognized by Fraenkel, but may be more clearly apparent in the visibly separated branches of the (R, c) -diagram than in the intricacies of his elliptic-function treatment.

The qualitative picture that emerges from these results and from a large number of further profile computations, is summarized by the sketch of figure 8, which is typical of any angular separation in the range $\frac{1}{2}\pi < 2\alpha < 2\alpha_c$. (If $2\alpha < \frac{1}{2}\pi$, the only qualitative change is that branch A passes through the origin with negative slope—cf. figure 5.) The velocity profiles on the various sections of branches A and B are as indicated, together with the code used by Fraenkel (1962) to distinguish the various classes. The

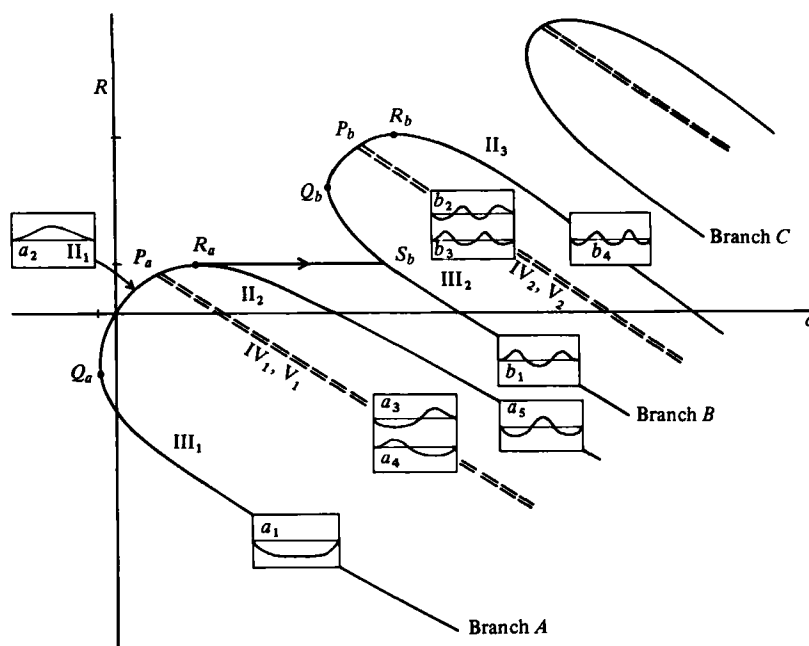


FIGURE 8. Qualitative character of velocity profiles on various sections of branches *A* and *B*, for $\frac{1}{2}\pi < 2\alpha < \pi$. The Roman numerals correspond to Fraenkel's (1962) classification. The classes change in a continuous manner at O and at P_a, P_b, \dots , and in a discontinuous manner at jumps such as $R_a \rightarrow S_b$.

dashed portions are drawn doubled, to indicate that there are two profiles (mirror images of each other) for each point.

Although we have numerically located only branches *A* and *B*, it is clear that these are merely the first two of an infinite sequence of branches *A, B, C, \dots* on which the profiles become progressively more complex. It is widely believed that the profiles of branches *B, C, \dots* are unstable, and attention is generally focused on the branch *A* profiles. The question of stability of branch *A* profiles may be related to the behaviour near the point R_a , and the fact that, if R is increased through R_a , a jump to a totally different profile is inevitable.

5.3. Behaviour of branches *A* and *B* for $0 < 2\alpha < 2\pi$

Figure 9(a) shows a sketch of the variation of branch *A* as 2α increases from 0 to $2\alpha_c \simeq 257.5^\circ$. The locus of the maximum R_a is indicated by the dashed curve.

For $2\alpha > 2\alpha_c$, as already observed, the linearized solution for small c is physically irrelevant, and the same may be true of the solution of (3.6) also. There is nevertheless some interest in continuing the sequence of curves of figure 9(a) beyond $2\alpha_c$, in order to provide a further point of contact with the results of Fraenkel (1962). This variation is shown in figure 9(b), which includes branch *B* also. When $2\alpha \simeq 266^\circ$, a fold develops in branch *A*, and, at a value $2\alpha_p$ between 266.7° and 267° , it merges with branch *B*, the topology of the branches changing at this critical angle. Defining R_a always as the Reynolds number at the maximum on the lower branch, R_a increases discontinuously at $2\alpha_p$, then decreases to zero at $2\alpha = 2\alpha'_c \simeq 282^\circ$, and then continues to decrease as 2α increases to 2π .

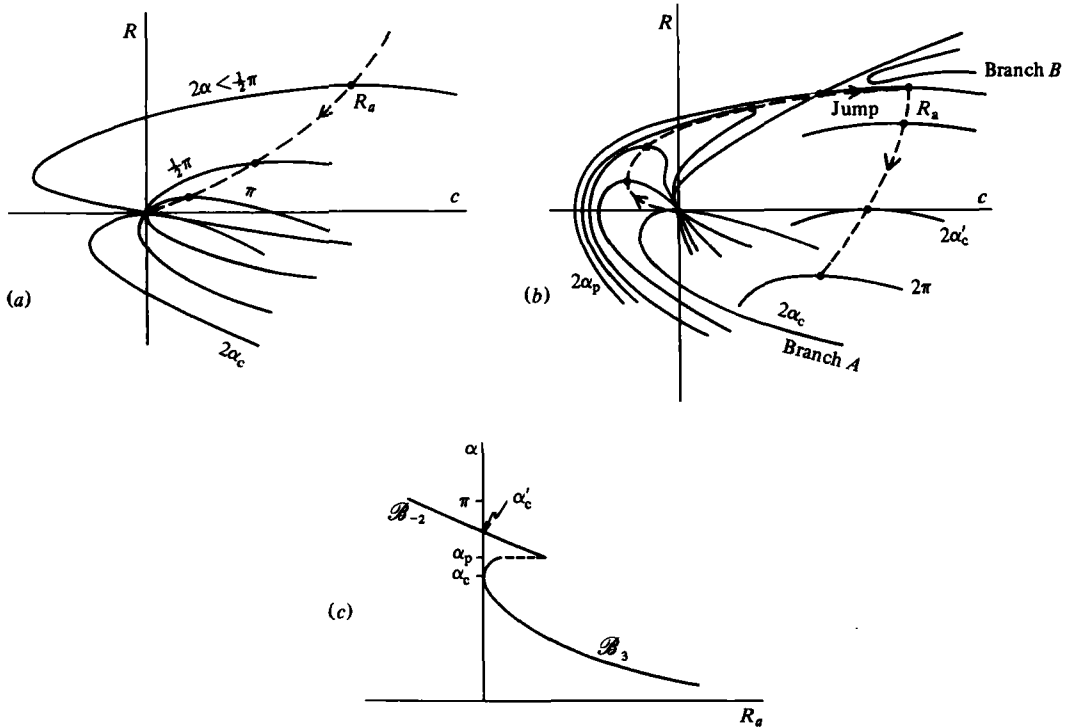


FIGURE 9. Sketch of the variation of branch A and its maximum R_a with α : (a) $0 < 2\alpha < 2\alpha_c$; (b) change in topology of branches A and B as 2α passes through $2\alpha_p \approx 266.8^\circ$; (c) inferred variation of R_a as a function of α .

The inferred qualitative variation of R_a over the full range $0-2\pi$ is shown in figure 9(c), in which the portions denoted $\mathcal{B}_3, \mathcal{B}_{-2}$ correspond to Fraenkel's (1962, figure 5) notation.

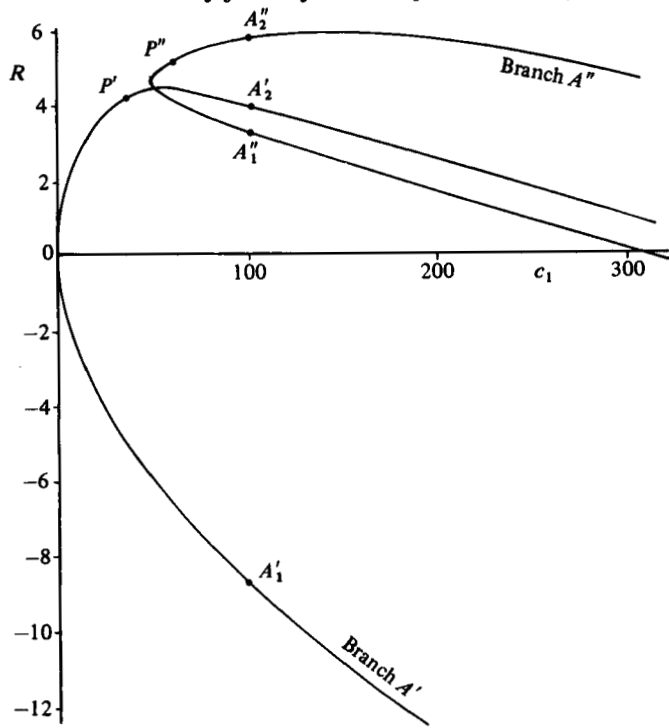
6. Numerical results for the two-fluid situation

We now return to the situation of § 4, in which there is a viscosity jump across $\theta = 0$. We may suppose, without loss of generality, that $\lambda = \mu_1/\mu_2 < 1$. In the discussion that follows, we focus attention on the change that occurs in branch A of the (R, c) -diagram as λ decreases from unity. Figure 10(a) shows what happens to branch A for the case $2\alpha = \frac{1}{2}\pi, \lambda = 0.9$; note that the abscissa here is the modified constant

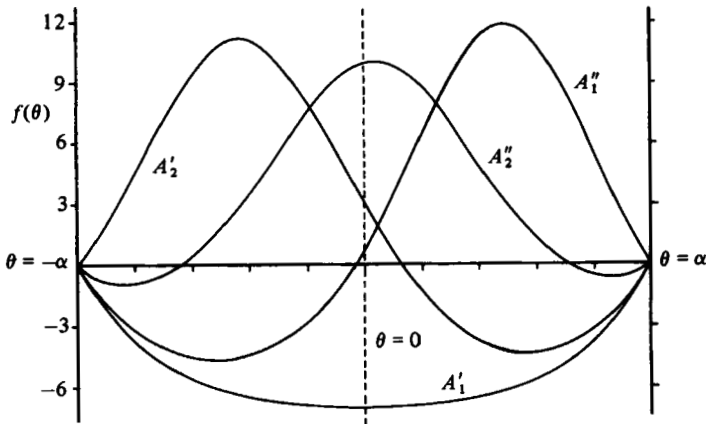
$$c_1 = \frac{(1 + \lambda)^2}{4\lambda^2} c. \tag{6.1}$$

The most striking effect is that we now have two intersecting branches, A' and A'' say, where A' passes through the origin, and A'' does not. Figure 10(b) shows the profiles corresponding to the points A'_1, A'_2, A''_1, A''_2 ($c_1 = 100$). A'_1 and A''_2 are nearly (but not exactly) symmetric about $\theta = 0$. The 'degeneracy' associated with the asymmetric flows when $\lambda = 1$ is clearly resolved when $\lambda \neq 1$.

The points P', P'' in figure 10(a) correspond to solutions for which $f'(\alpha) = 0$. As R increases through $R(P')$, the flow changes from purely divergent flow to a flow of



(a)



(b)

FIGURE 10. (a) Modification of branch A for $2\alpha = \frac{1}{2}\pi$ when $\lambda = 0.9$: the branch splits into two branches, A' and A'' ; the points P' and P'' correspond to profiles with zero gradient on $\theta = \alpha$. (b) Velocity profiles for $\lambda = 0.9$ corresponding to the points A'_1, A'_2, A''_1, A''_2 on branches A' and A'' .

type A'_2 (divergent but with inflow near the wall in the less viscous fluid). Similarly, as R increases through $R(P'')$, the flow changes from type A''_1 (inflow in the more viscous fluid) to one of type A''_2 with inflow on both walls. It seems likely that at least one of the flows A'_2, A''_1, A''_2 (probably A'_2) is structurally unstable.

On branch A' , there is again a maximum value of R , R'_a say, and now if R is increased slowly from 0 through R'_a , the flow will (presumably) jump from branch A' to branch

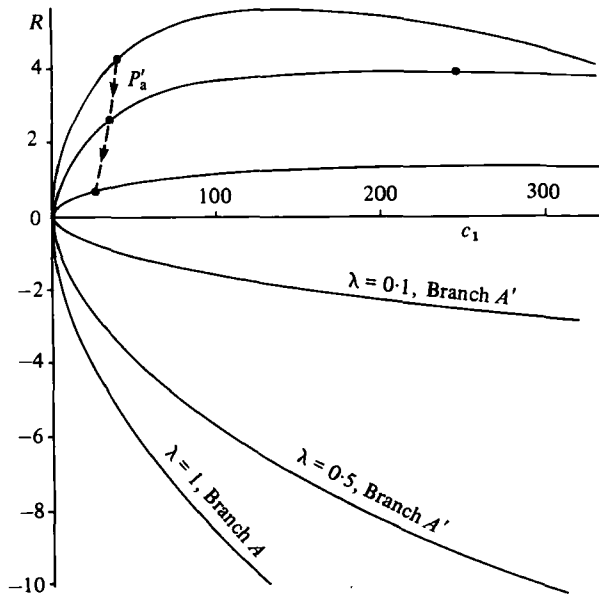


FIGURE 11. Change in branch A' as λ decreases. The abscissa is $c_1 = \frac{1}{2}(1 + \lambda^{-1})^2 c$.

A'' . If R is increased further, a second jump will occur (presumably to branch B') when $R = R''_a$, the maximum on branch A'' .

Figure 11 shows the effect on branch A' of a further decrease in λ . As λ decreases, R'_a decreases (and the value of c_1 where the maximum occurs increases quite rapidly). The value of R at which reversed flow appears also decreases as indicated in the figure.

When R is large and negative, we again expect the solutions (on branch A') to have a boundary-layer character near each wall, with boundary-layer thicknesses proportional to $\mu_1^{\frac{1}{2}}$ and $\mu_2^{\frac{1}{2}}$ in the two fluids. For the region near $\theta = \alpha$, an analysis similar to that in § 5.1 shows that, for large c ,

$$f(\theta) \sim K^2 f_0(\eta) + \tilde{\mu}_1 f_1(\eta), \quad \eta = \tilde{\mu}_1^{-\frac{1}{2}} K(\alpha - \theta), \tag{6.2}$$

where $K = (\frac{1}{2}c)^{\frac{1}{2}}$, and f_0 and f_1 are given by (5.13) and (5.15). There is a similar structure near $\theta = -\alpha$. At leading order, the flow outside the boundary layers is effectively the 'inviscid' flow associated with a line sink ($Q < 0$). Across $\theta = 0$, the $O(K^2)$ solutions in the two fluids match with zero shear stress: the effectively inviscid flow is indifferent to a jump in viscosity at $\theta = 0$. Continuing to next order, we have, well away from the walls,

$$f(\theta) \sim \begin{cases} -K^2 - \tilde{\mu}_1 & (\theta > 0), \\ -K^2 - \tilde{\mu}_2 & (\theta < 0), \end{cases} \tag{6.3}$$

indicating that there must be a weak (i.e. $O(1)$) shear layer at the interface. A straightforward analysis shows that, near $\theta = 0$,

$$f(\theta) \sim \begin{cases} -K^2 - \tilde{\mu}_1(1 + A_1 e^{-2\eta_1}), & \eta_1 = \tilde{\mu}_1^{-\frac{1}{2}} K\theta \quad (\theta \geq 0), \\ -K^2 - \tilde{\mu}_2(1 + A_2 e^{-2\eta_2}), & \eta_2 = -\tilde{\mu}_2^{-\frac{1}{2}} K\theta \quad (\theta \leq 0), \end{cases} \tag{6.4}$$

with $A_1 = \lambda^{-1} - \lambda^{-\frac{1}{2}}$, $A_2 = \lambda - \lambda^{\frac{1}{2}}$. Figures 12(a, b) show velocity profiles for $c_1 = 10^5$, 10^6 for a range of values of λ (for $2\alpha = 10^\circ$). As expected, the velocity gradient is

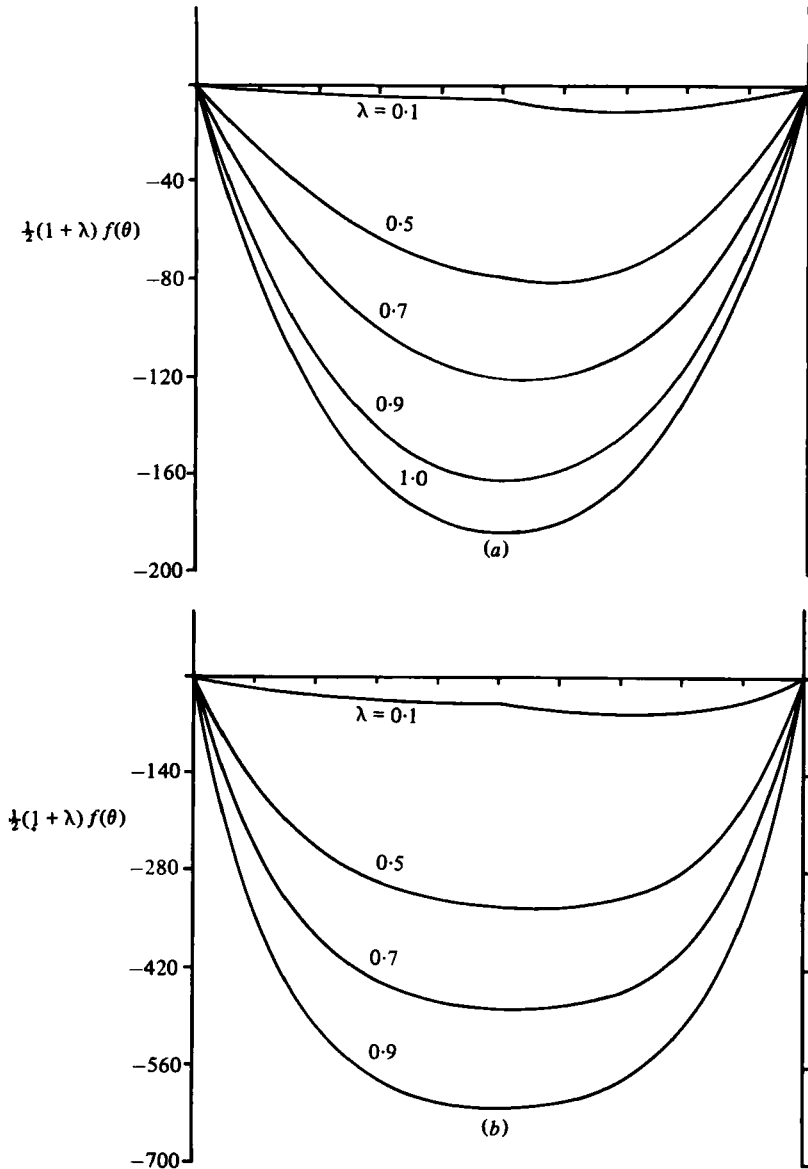


FIGURE 12. Velocity profiles for $2\alpha = 10^\circ$, and various values of λ . (a) $c_1 = 10^5$; (b) $c_1 = 10^6$. The jump in velocity gradient at $\theta = 0$ is scarcely detectable for $\lambda > 0.5$.

almost continuous across $\theta = 0$, consistent with the above argument. (The strong decrease in flux as λ decreases is associated with the corresponding reduction in c , given by (6.1): e.g., when $\lambda = 0.1$, $c = 3.3 \times 10^{-2}c_1$.)

Finally, we have investigated the behaviour of the branches A' and A'' as λ decreases (for fixed α) to the value for which $\alpha = \alpha_{c_1}(\lambda)$ ($E \rightarrow F$ in figure 3a). With $2\alpha = 150^\circ$, the critical value of λ given by (4.11) is 0.228 ; figure 13 shows the computed behaviour as λ decreases from 0.27 to 0.228 . For $\lambda = 0.27$, the branches A' and A'' still cross (at the point V in the figure), but at $\lambda = 0.265$ the curves have 'pinched off', forming two new branches \tilde{A}' and \tilde{A}'' . At this value of λ , there is no solution (on these branches)

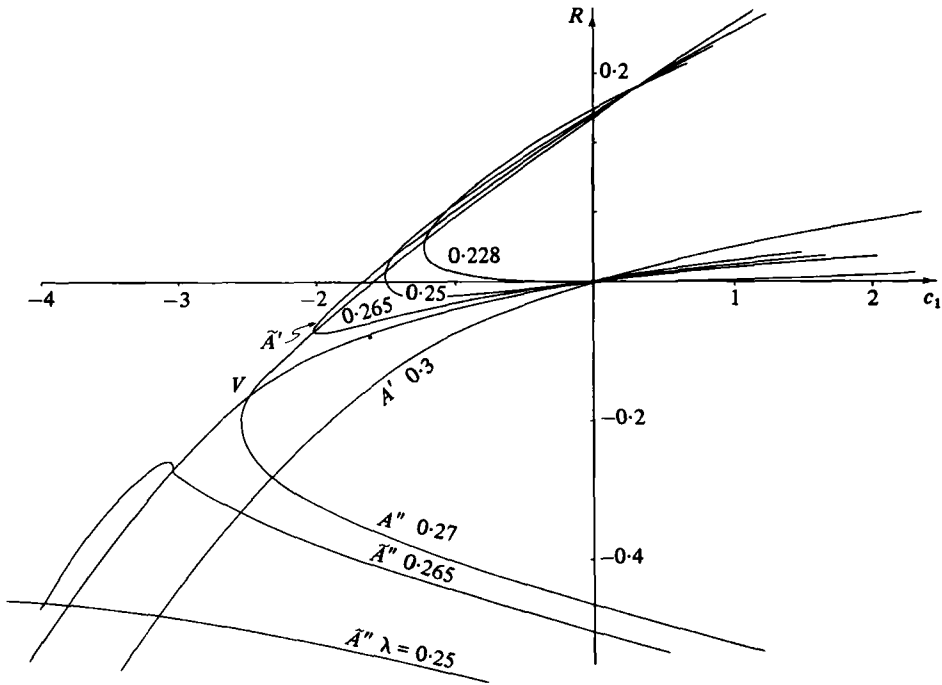


FIGURE 13. Change in branches A' and A'' for $2\alpha = 150^\circ$ as λ decreases from 0.27 to 0.228 (cf. figure 3). At a value of λ between 0.27 and 0.265, the branches split (near V) forming two new branches \tilde{A}' and \tilde{A}'' which move apart with further reduction of λ . For $\lambda = 0.228$, branch \tilde{A}' touches the axis $R = 0$ at $c = 0$.

with $-0.27 < R < -0.08$. As λ is decreased further, \tilde{A}' and \tilde{A}'' move further apart, until (when $\lambda = 0.228$) \tilde{A}'' lies in $R < -0.66$ and \tilde{A}' lies in $R > 0$, with a minimum at O (consistent with (4.11) at the critical value of λ).

7. Discussion

The foregoing analysis enables us (in principle) to determine the position of the interface in such situations as those sketched in figure 14(a, b), even when $|R\alpha|$ is not small. We have seen in § 2 that, when $|R\alpha| \ll 1$, the interface positions itself so that the ratio of fluid widths is constant. When $|R\alpha| \gg 1$, the situation is very different. For example, in the situation of figure 14(a), when $|R\alpha| \gg 1$, the two fluxes Q_1 and Q_2 are equal (apart from boundary-layer corrections) and so the position of the interface in the straight section is determined by (2.16) with $q = 1$. As $\lambda \rightarrow 0$, $H \rightarrow 1$, i.e. the interface moves towards the upper boundary.

Similarly if Q_1 and Q_2 are specified, then the position of the interface in the straight section is determined by (2.16), and its position $\theta = \beta$ in the adjacent converging or diverging section (as, for example, in figure 14b) is, in principle, determinate from numerical solution of the Jeffery-Hamel problem.

There is of course an important question concerning the stability of the various steady flows described in this paper. Instabilities may be of three types. First, there is the conventional instability of flows exhibiting points of inflexion, which may be expected at quite low Reynolds numbers ($R \gtrsim 20$). The methods of Eagles (1966)

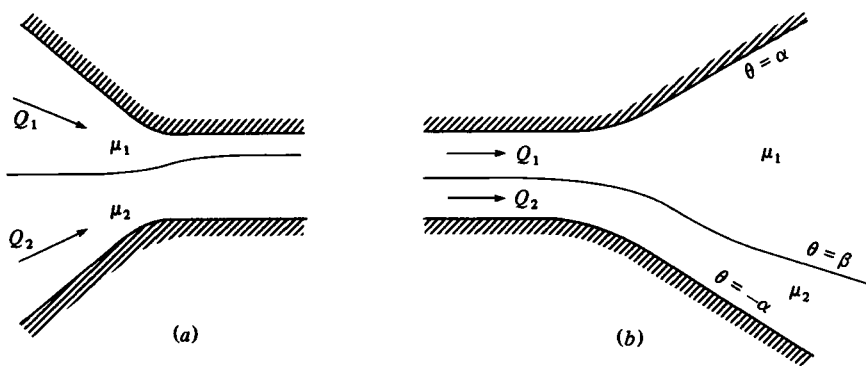


FIGURE 14. Determination of the asymptotic position of the interface: (a) a case of converging flow entering a uniform section; (b) a case of flow entering a diverging section. In both cases the downstream position of the interface is determined in principle by the values of $q = Q_1/Q_2$ and $\lambda = \mu_1/\mu_2$. In both cases, the figure is schematic, and is not intended to imply that a solution has been found which describes the flow through the transition region, which may be extensive when the Reynolds number is not small.

could perhaps be extended to cover the two-fluid situation. Secondly, there is the instability associated specifically with viscosity stratification, discovered by Yih (1967); this is a long-wavelength instability, involving inertial effects, but which nevertheless persists at arbitrarily small R . The physical mechanism of this instability is as yet obscure, and it is by no means clear how it may be affected by weak convergence or divergence of the fluid boundaries.

Finally, there is the question of structural stability (in the sense of bifurcation theory) already alluded to in § 6. If we imagine the steady problem (3.5) imbedded in the wider class of unsteady problems (with the same boundary conditions)

$$\frac{\partial f}{\partial t} + (\tilde{\mu}f')' + 4\tilde{\mu}f + 2\tilde{\beta}f^2 = c, \tag{7.1}$$

then the steady solutions obtained above may be unstable to perturbations $\delta f(\theta, t)$. On general grounds (Benjamin 1976) one would expect approximately half of the multiplicity of flows at a given Reynolds number to be structurally unstable; an associated hysteresis behaviour in increasing and decreasing the Reynolds number through a range of positive values may be anticipated.

These various stability aspects perhaps deserve further study.

This work has been partially supported by the Science Research Council under Research Grant no. GR/A/5993.4. We gladly acknowledge the penetrating comments of L. E. Fraenkel on an earlier version of this paper.

REFERENCES

BARENBLATT, G. I. & ZEL'DOVICH, YA. B. 1972 Self-similar solutions as intermediate asymptotics. *Ann. Rev. Fluid Mech.* **4**, 285.
 BATCHELOR, G. K. 1967 *An Introduction to Fluid Dynamics*. Cambridge University Press.
 BENJAMIN, T. B. 1976 Applications of Leray-Schauder degree theory to problems of hydrodynamic stability. *Math. Proc. Camb. Phil. Soc.* **79**, 383.
 BULAKH, B. M. 1964 On higher approximations in the boundary-layer theory. *J. Appl. Math. Mech.* **28**, 675.

- EAGLES, P. M. 1966 The stability of a family of Jeffery–Hamel solutions for divergent channel flow. *J. Fluid Mech.* **24**, 191.
- FRAENKEL, L. E. 1962 Laminar flow in symmetrical channels with slightly curved walls. I. On the Jeffery–Hamel solutions for flow between plane walls. *Proc. R. Soc. Lond. A* **267**, 119.
- GOLDSTEIN, S. 1938 *Modern Developments in Fluid Dynamics*, vol. 1. Clarendon.
- HAMEL, G. 1916 Spiralförmige Bewegungen zäher Flüssigkeiten. *Jahresbericht der Deutschen Math. Vereinigung.* **25**, 34.
- JEFFERY, G. B. 1915 Steady motion of a viscous fluid. *Phil. Mag. Ser. 6*, **29**, 455.
- MILLSAPS, K. & POHLHAUSEN, K. 1953 Thermal distributions in Jeffery–Hamel flows between non-parallel plane walls. *J. Aero. Res.* **20**, 187.
- MOFFATT, H. K. & DUFFY, B. R. 1980 Local similarity solutions and their limitations. *J. Fluid Mech.* **96**, 299.
- ROSENHEAD, L. 1940 The steady two-dimensional radial flow of viscous fluid between two inclined walls. *Proc. R. Soc. Lond.* **175**, 436.
- YIH, C.-S. 1967 Instability due to viscosity stratification. *J. Fluid Mech.* **27**, 337.